

2

REPORT SSD-TR-90-28

AD-A229 444

DTIC FILE COPY

Direct Observation of NF(X) Using Laser Induced Fluorescence: Determination of the H + NF₂ Branching Ratio

Prepared by

R. F. HEIDNER III, H. HELVAJIAN, J. S. HOLLOWAY, and J. B. KOFFEND
Aerophysics Laboratory
Laboratory Operations
The Aerospace Corporation
El Segundo, CA 90245-4691

30 September 1990

Prepared for

SPACE SYSTEMS DIVISION
AIR FORCE SYSTEMS COMMAND
Los Angeles Air Force Base
P.O. Box 92960
Los Angeles, CA 90009-2960

DTIC
ELECTE
NOV 20 1990
S B D
C/c


APPROVED FOR PUBLIC RELEASE;
DISTRIBUTION UNLIMITED

90 11 19 27 6

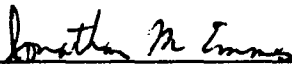
This report was submitted by The Aerospace Corporation, El Segundo, CA 90245, under Contract No. F04701-88-C-0089 with the Space Systems Division, P.O. Box 92960, Los Angeles, CA 90009-2960. It was reviewed and approved for The Aerospace Corporation by R. W. Fillers, Director, Aerophysics Laboratory. Capt Riviere was the project officer for the Mission-Oriented Investigation and Experimentation (MOIE) Program.

This report has been reviewed by the Public Affairs Office (PAS) and is releasable to the National Technical Information Service (NTIS). At NTIS, it will be available to the general public, including foreign nationals.

This technical report has been reviewed and is approved for publication. Publication of this report does not constitute Air Force approval of the report's findings or conclusions. It is published only for the exchange and stimulation of ideas.



RAFAEL A. RIVIERE, Capt, USAF
MOIE Project Officer
SSD/CNL



JONATHAN M. EMMES, Maj, USAF
MOIE Program Manager
AFSTC/WCO OL-AB



REPORT DOCUMENTATION PAGE

1a. REPORT SECURITY CLASSIFICATION Unclassified		1b. RESTRICTIVE MARKINGS	
2a. SECURITY CLASSIFICATION AUTHORITY		3. DISTRIBUTION/AVAILABILITY OF REPORT Approved for public release; distribution unlimited.	
2b. DECLASSIFICATION/DOWNGRADING SCHEDULE		4. PERFORMING ORGANIZATION REPORT NUMBER(S) TR-0090(5930-04)-2	
5. MONITORING ORGANIZATION REPORT NUMBER(S) SSD-TR-90-28		6a. NAME OF PERFORMING ORGANIZATION The Aerospace Corporation Laboratory Operations	
6b. OFFICE SYMBOL (If applicable)		7a. NAME OF MONITORING ORGANIZATION Space Systems Division	
6c. ADDRESS (City, State, and ZIP Code) El Segundo, CA 90245-4691		7b. ADDRESS (City, State, and ZIP Code) Los Angeles Air Force Base Los Angeles, CA 90009-2960	
8a. NAME OF FUNDING/SPONSORING ORGANIZATION		8b. OFFICE SYMBOL (If applicable)	
9. PROCUREMENT INSTRUMENT IDENTIFICATION NUMBER F04701-88-C-0089		10. SOURCE OF FUNDING NUMBERS	
8c. ADDRESS (City, State, and ZIP Code)		PROGRAM ELEMENT NO.	PROJECT NO.
		TASK NO.	WORK UNIT ACCESSION NO.
11. TITLE (Include Security Classification) Direct Observation of $NF(X)$ Using Laser Induced Fluorescence: Determination of the $H + NF_2$ Branching Ratio			
12. PERSONAL AUTHOR(S) Heidner III, Raymond F.; Helvajian, Henry; Holloway, John S.; and Koffend, John B.			
13a. TYPE OF REPORT	13b. TIME COVERED FROM _____ TO _____	14. DATE OF REPORT (Year, Month, Day) 1990 September 30	15. PAGE COUNT 29
16. SUPPLEMENTARY NOTATION.			
17. COSATI CODES		18. SUBJECT TERMS (Continue on reverse if necessary and identify by block number)	
FIELD	GROUP	SUB-GROUP	Chemical lasers
			Nitrogen fluoride
			Electronic excitation
			Photolysis
			Nitrogen difluoride
			Quantum yield
19. ABSTRACT (Continue on reverse if necessary and identify by block number) <i>19(1) to 19(2) delete -</i> For the first time, the branching ratio for the $H + NF_2^+$ has been measured using direct detection of the excited $NF(a^1\Delta)$ and the ground $NF(X^3\Sigma^-)$ states. $NF(a^1\Delta)$ was observed by its emission at 874 nm from both the 249 nm photolysis of NF_2 and from the reaction of H atoms (produced from HBr photolysis at 193 nm) with NF_2^+ . While $NF(X^3\Sigma^-)$ was easily detected by laser induced fluorescence on the $NF b^1\Sigma^- - X^3\Sigma^-$ transition following 249 nm NF_2^+ photolysis, it was not observed following the $H + NF_2^+$ reaction. This result leads to a lower limit for the $NF(a)$ branching ratio, $NF(a)/NF_{tot} > 0.90 \pm 0.03$, in accord with previous results. The measured $NF(a^1\Delta)$ quantum yield from KrF photolysis of NF_2^+ , $\Phi_{NF(a)} < 0.04 \pm 0.02$, also agrees with prior work. The NF_2^+ photolysis quantum yield is observed to be unity, based on results from an HCl titration of the F atoms from the 249 nm photolysis of NF_2^+ . <i>19(1) to 19(2) delete -</i>			
20. DISTRIBUTION/AVAILABILITY OF ABSTRACT <input checked="" type="checkbox"/> UNCLASSIFIED/UNLIMITED <input type="checkbox"/> SAME AS RPT. <input type="checkbox"/> DTIC USERS		21. ABSTRACT SECURITY CLASSIFICATION Unclassified	
22a. NAME OF RESPONSIBLE INDIVIDUAL		22b. TELEPHONE (Include Area Code)	22c. OFFICE SYMBOL

CONTENTS

I. INTRODUCTION..... 5

II. EXPERIMENTAL..... 7

III. RESULTS AND DISCUSSION..... 11

A. NF_2 Photolysis Quantum Yield..... 11

B. $\text{NF}(a)$ Branching Fraction..... 12

IV. CONCLUSIONS..... 25

REFERENCES..... 27



Accession For	
NTIS GRA&I	<input checked="" type="checkbox"/>
DTIC TAB	<input type="checkbox"/>
Unannounced	<input type="checkbox"/>
Justification	
By _____	
Distribution/	
Availability Codes	
Dist	Avail and/or Special
A-1	

FIGURES

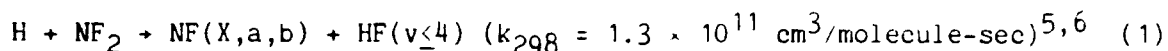
1.	Diagram of the Experimental Apparatus.....	8
2.	Results of the HCl Titration of F Atoms from the KrF Laser Photolysis of NF_2	13
3.	Plots of the NF b-X LIF Intensity as a Function of Laser Energy.....	16
4.	(a) Plot of the NF(a) Amplitude from the 193 nm Photolysis of HBr in the Presence of NF_2 ; (b) Plot of the NF(a) Amplitude from the 249 nm Photolysis of NF_2	18
5.	Plot of the NF b-X LIF Amplitude as a Function of $[\text{NF}_2]$ from the KrF Laser Photolysis of NF_2	19
6.	(a) Time Profiles of NF b-X LIF Intensity Obtained by Tuning the Dye Laser to the $\text{Q}_P(9)/\text{Q}_R(9)$ Line of the (0,0) Band and Varying the Delay Between the Excimer Laser and Dye Laser Pulses; (b) NF b-X Excitation Spectra Obtained by Fixing the Delay Between the Excimer and Dye Lasers to 15 μsec and Scanning the Dye Laser Wavelength.....	20
7.	Time Profiles of NF b-X LIF Intensity Obtained by Tuning the Dye Laser to the $\text{Q}_P(9)/\text{Q}_R(9)$ Line of the (0,0) Band and Varying the Delay Between the Excimer Laser and Dye Laser Pulses.....	22

TABLE

1.	Experimental NF b-X LIF and a-X Emission Amplitudes vs Density.....	23
----	--	----

I. INTRODUCTION

The rapid reaction of hydrogen atoms with the NF_2 radical



is among very few that produce electronically excited products in high yield.¹⁻⁷ The production of the $\text{NF}(a^1\Delta)$ radical has been cited as the dominant channel.^{6,7} It has been suggested^{1,4} that this reaction proceeds via an addition-elimination mechanism forming HNF_2 as the intermediate. Since the triplet surface leading on the entrance channel is expected to be repulsive, the reaction occurs via the HNF_2 1A surface, and spin considerations preclude formation of triplet NF . The abstraction reaction, however, favors the production of $\text{NF}(X^3\Sigma^-)$.⁴ Several indirect measurements of the $\text{NF}(a^1\Delta)$ branching ratio have been performed. Cheah and Clyne⁶ monitored time profiles of N atoms produced from the H/NF_2 system and, using spin conservation arguments, conclude that the $\text{NF}(a^1\Delta)$ branching fraction is in excess of 90%. Their results stem from the fact that $\text{N}(^4S)$, produced primarily from the reaction of H and $\text{NF}(X^3\Sigma^-)$, was not observed at early times during the reaction. Malins and Setser⁷ also report a large $\text{NF}(a^1\Delta)$ branching ratio of 91%. Their results are based upon relative emission intensity measurements of $\text{HF}(v = 4)$, whose formation is energetically allowed only for the $\text{NF}(X^3\Sigma^-)$ channel. They also examined the vibrational distributions of the NF and HF products, and their RRKM analysis supports an addition-elimination reaction mechanism. More recently,⁸ however, absolute photometry measurements were performed on the $\text{H} + \text{NF}_2$ flame in a flow tube reactor. It was determined that the $\text{NF}(a^1\Delta)$ yield, under hydrogen-rich conditions, is only 15-30% of the initial NF_2 density.

We have performed a direct determination of the $\text{NF}(a^1\Delta)$ branching fraction using a technique that does not depend upon absolute detectivity calibrations. Relative amplitudes of both $\text{NF}(a^1\Delta)$ and $\text{NF}(X^3\Sigma^-)$ produced from the 249 nm photolysis of NF_2 and from the $\text{H} + \text{NF}_2$ reaction have been measured

using emission spectroscopy and laser induced fluorescence (LIF), respectively. The $H + NF_2$ reaction was studied by the ArF photolysis of HBr to create H atoms in the presence of NF_2 . A knowledge of the NF_2 absorption cross section at 249 nm and the HBr cross section at 193 nm allows the extraction of the absolute $NF(a^1\Delta)$ yield from the experimental data, since the experimental geometry was held fixed throughout the experiment. In addition, any loss of NF_2 during its transport through the gas handling system to the observation region does not affect our results. Such a loss of NF_2 , possibly due to wall assisted NF_2 disproportionation, may explain the low $NF(a^1\Delta)$ yield reported in ref. 8.

II. EXPERIMENTAL

NF_2 and HBr were photolyzed using a Lumonics 400 Hyperex excimer laser operating with KrF (249 nm) or ArF (193 nm), respectively. The excimer beam was directed into the photolysis cell through a series of beam shaping lenses. Two slit apertures were placed in the beam path to minimize scattered excimer light. A Quantel Datachrome 581C Nd:YAG pumped dye laser system operating with Coumarin 500 dye provided tunable radiation to probe the NF b-X transition near 530 nm. Baffles on the dye laser entrance arm of the cell helped reduce scattered dye laser light. Uncoated Suprasil windows were used to provide small fractions of the dye and excimer beams for relative laser energy measurements, obtained from a silicon photodiode and a Laser Precision RJP-734 energy meter, respectively. The relative response of the energy meter for the KrF and ArF wavelengths was performed in situ using a large area (5 in. diam) calorimetric power meter that had been previously calibrated. The exit window of the photolysis cell was removed, and the large power meter sampled the entire excimer beam for these measurements. The energy meter was absolutely calibrated in the same manner for the HCl titration experiments described below. A Lasertechnics model 100F Fizeau wavemeter served to determine the wavelength of the dye laser. A diagram of the experimental arrangement is shown in Fig. 1.

The gases in these experiments used without further purification were CO_2 (Matheson 99.99%), Ar (Matheson 99.99%), SF_6 (MG Gases 99.9%), and N_2F_4 (Hercules 96%). HCl (Matheson 99.0%) and HBr (Matheson 99.8%) were first cooled to liquid nitrogen temperatures and pumped to remove any free H_2 . They were then vacuum distilled to remove any Br_2 or Cl_2 . The purified HBr or HCl was mixed with Ar and stored at 1000 Torr in a Teflon coated reservoir. Mixtures of N_2F_4 in argon were prepared and stored at 100 psia in a stainless steel reservoir. Reagents were flowed into the photolysis cell through calibrated Tylan flowmeters. The cell, constructed of stainless steel and internally Teflon coated, was wrapped in heating tape and maintained at 145°C . At this temperature, the N_2F_4 is >95% dissociated into NF_2^{9-13} for the

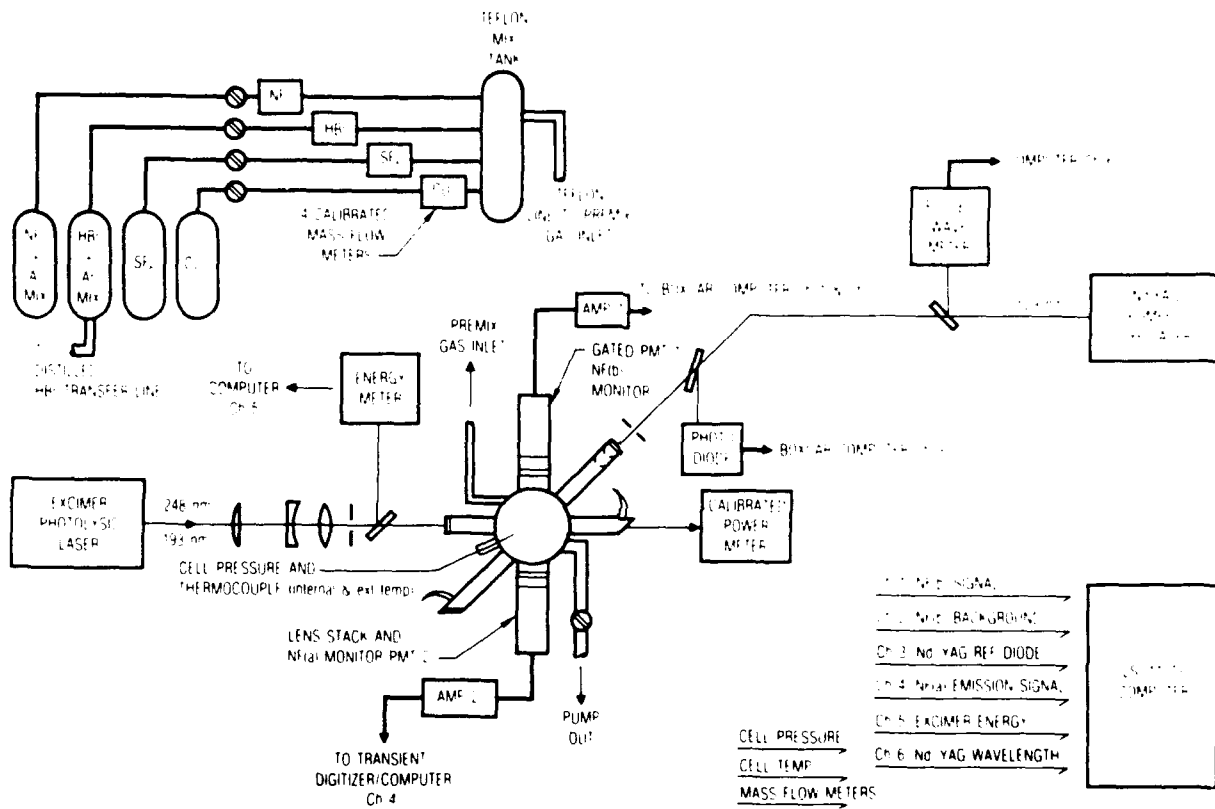


Fig. 1. Diagram of the Experimental Apparatus.

NF₂ densities used in these experiments. Cell pressure was measured with an MKS Baratron capacitance manometer.

NF(a) was monitored with a GaAs photomultiplier tube viewing the NF a-X emission through a 1 nm full-width at half-maximum (FWHM) interference filter centered at 874.3 nm. For the F atom titration experiments, emission of the HF 2-0 overtone was observed using a LN₂ cooled intrinsic Ge detector through a 1270 nm interference filter (30 nm FWHM). The GaAs or Ge detector output was amplified and processed with a LeCroy model 2264 transient digitizer whose output was averaged and stored in a DEC 11/23 computer. The NF b-X LIF was detected with a gatable EMI 9816QB photomultiplier (PMT) tube mounted on one arm of the photolysis cell. A 1 nm FWHM filter centered at 528.9 nm was used to isolate part of the NF b-X (0,0) band near the strong Q_P/Q_R head. Since the strong NF b-X vibronic bands are diagonal in vibrational quantum number¹⁴⁻¹⁶ ($q_{00} = 0.96$),¹⁴ it was essential to gate the photomultiplier off during the dye laser probe pulse to eliminate scattered dye laser radiation.

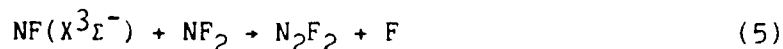
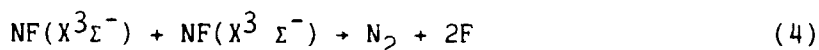
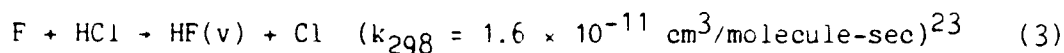
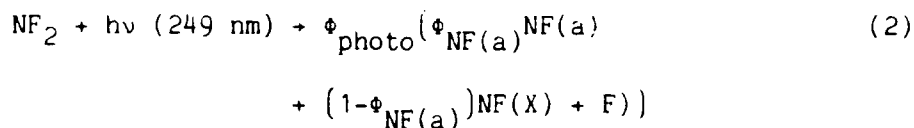
We observed a signal from the NF b-X phototube in the absence of the dye laser. This background is primarily due to cell window fluorescence caused by scattered excimer light in addition to NF b-X chemiluminescence from the NF₂ photolysis¹⁷ and from the H + NF₂ reaction.⁷ The b-X signal is ultimately traceable to NF(a¹Δ) + HF(v) E-V energy pooling. The excimer laser was operated at a repetition rate of 10 Hz, while the dye laser was pulsed at 5 Hz. The dye laser was synchronized to fire upon every other excimer laser shot, and dual channel detection was employed in order to perform background subtraction. The PMT output was sent into a Tektronix AM-502 amplifier and processed using two channels of an SRS Si250 boxcar integrator. One channel is triggered at 5 Hz, in phase with the dye laser, and acquires the NF b-X LIF signal. The second boxcar, also triggered at 5 Hz but out of phase with the dye laser, obtains the signal due to the excimer laser alone. The two boxcar outputs were digitized and recorded with a DEC 11/73 laboratory computer. The relative dye laser and excimer laser energy measurements were also acquired using the computer. A third boxcar was used for the dye laser, while the analog output from the energy meter was used directly.

$\text{NF}(X^3\Sigma^-)$ time profiles were generated by scanning the delay between the excimer laser photolysis and the dye laser probe pulses, while the $\text{NF}(a^1\Delta)$ and $\text{HF}(v = 2)$ time behavior was obtained directly using the transient digitizer. Throughout this study, NF b-X LIF was excited by tuning the dye laser to the $Q_P(9)/Q_R(9)$ line of the (0,0) band at 18909.29 cm^{-1} . The pulsed wavemeter was used to adjust the laser's frequency to line center. In all cases, final adjustment was made by maximizing the NF b-X LIF signal in real time. In the case of the ArF photolysis of HBr/NF_2 mixtures where no LIF was detected, the ArF laser was blocked, and 266 nm radiation was directed into the cell to create $\text{NF}(X^3\Sigma^-)$ from NF_2 photolysis for peaking up the LIF signal prior to each run. The 266 nm radiation was produced by frequency doubling the excess 532 nm light from the YAG laser system. The $\text{NF}(X^3\Sigma^-)$ quantum yield is nearly 99% at 266 nm¹⁸ and near the peak of the 266 nm absorption band at 260 nm.¹⁸⁻²⁰ Extreme care was taken to ensure that the detection geometry was held constant for the experiments which investigated relative $\text{NF}(a^1\Delta)$ and $\text{NF}(X^3\Sigma^-)$ yields from the KrF photolysis of NF_2 and those which probed the branching ratio from the ArF photolysis of HBr/NF_2 mixtures.

III. RESULTS AND DISCUSSION

A. NF₂ PHOTOLYSIS QUANTUM YIELD

The first absorption band of NF₂ at 260 nm exhibits diffuse structure.^{18,19} Under 0.25 cm⁻¹ resolution,¹⁸ no additional structure is observed, and the features are probably indicative of the excited NF₂ electronic surface and dissociation process, analogous to O₃ photolysis in the Hartley bands.²¹ Previous work in this laboratory^{17,18} has shown that following UV NF₂ photolysis, the appearance of the NF(a¹Δ) fragment occurs on a time scale of 80 μsec. In contrast, the NF(X³Σ⁻) photofragment was recently observed to be produced promptly,²² which is behavior more in accord with continuum dissociation. In light of these data, however, an argument could be made for a short lived NF₂ excited state playing a role in its dissociation. Although the NF(a¹Δ) photolysis quantum yield is only 10±5%¹⁷ at 249 nm, the question is raised whether the NF₂ photolysis yield is unity, an assumption inherent in the data analysis presented below. In order to measure the photolysis yield, an HCl titration of the F atoms from the KrF photolysis of NF₂ was undertaken. The following reactions must be considered for the titration:



where ϕ_{photo} is the NF₂ photolysis yield and $\phi_{\text{NF(a)}}$ is the fraction of dissociation events yielding NF(a). We see from Eqs. (4) and (5) that any NF(X³Σ⁻) formed results in an additional F atom created either from

bimolecular disproportionation^{5,6} or by reaction with NF_2 .²² Any direct reaction of $\text{NF}(a^1\Delta)$ or electronic quenching resulting in F atom production can be neglected under our experimental conditions.^{17,24} Hence, each photon absorbed by NF_2 results in the formation of $\phi_{\text{photo}} [1 + (1 - \phi_{\text{NF}(a)})]$ fluorine atoms.

In a series of experiments, NF_2 HCl-Ar mixtures were photolyzed using a KrF laser. The total pressure and NF_2 density were held constant, and the HCl partial pressure was varied, while time profiles of $\text{HF}(v = 2)$ were recorded using the $\text{HF}(2-0)$ overtone emission near 1270 nm. The $\text{HF}(v = 2)$ time profiles were fit to a rising and falling double exponential to obtain amplitudes. Figure 2 shows a set of $\text{HF}(v = 2)$ emission amplitudes plotted as a function of HCl density. Also shown is the calculated titration point with $\phi_{\text{photo}} = 1$ and the NF_2 absorption cross section reported in Ref. 18. The major source of the estimated error in the calculation is due to the uncertainty in determination of the KrF beam area. However, there is good agreement between the experiment and the calculation. We repeated the titration using a different NF_2 density with similar results. We conclude, within an estimated error of 20%, that NF_2 dissociates with unit quantum efficiency at 249 nm.

B. NF(a) BRANCHING FRACTION

The reaction of H atoms with NF_2 yields an NF molecule and an HF molecule.^{5,6} The NF product is formed in either the $X^3\Sigma^-$, $a^1\Delta$, or the $b^1\Sigma$ state. Malins and Setser⁷ report $\text{NF}(X):\text{NF}(a):\text{NF}(b)$ branching fractions of 0.07:0.91:0.02. Their value of 2% for the $\text{NF}(b)$ state yield is based upon the 200 msec $\text{NF } b-X$ radiative lifetime reported by Clyne and White.² Subsequent work²⁵⁻²⁸ has shown that the $b-X$ radiative lifetime is a factor of 10 shorter. Thus, the $\text{NF}(b)$ branching fraction is lowered to 0.2%, and it can be effectively neglected. Our ability to probe both the $\text{NF}(X)$ and $\text{NF}(a)$ states enables us to perform a direct determination of the $\text{H} + \text{NF}_2$ reaction branching ratio without the need for absolute calibration. The $\text{NF } b-X$ LIF and $\text{NF } a-X$ emission signal amplitudes, normalized for KrF laser flux, from the photolysis of NF_2 , are given by

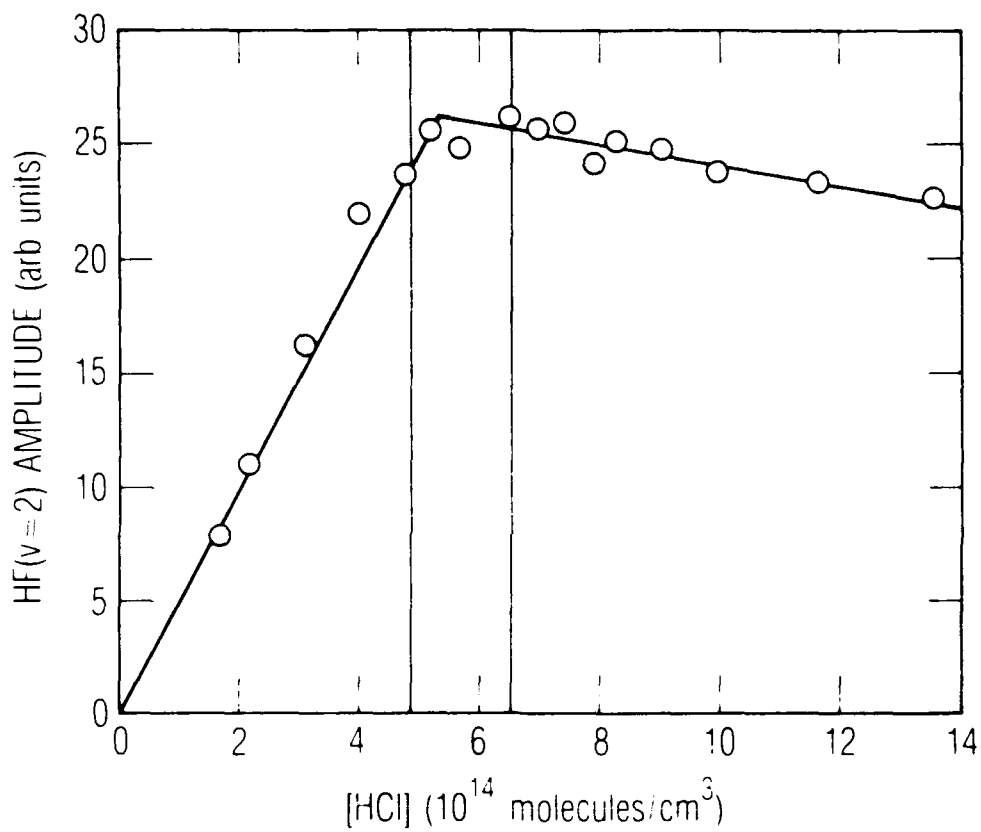


Fig. 2. Results of the HCl titration of F Atoms from the KrF Laser Photolysis of NF_2 . The NF_2 density was held constant at 5.0×10^{15} molecules/cm 3 , and the NF_2 photolysis fraction was $6 \pm 1\%$. The vertical lines indicate the calculated titration point of 5.7×10^{14} molecules/cm 3 using an $\text{NF}(X)$ photolysis quantum yield of 90% (see text).

$$S_{a-X}/I_{249} = F_{a-X} \phi_a \sigma_{249} [NF_2] \quad (6)$$

and

$$S_{b-X}/I_{249} = F_{b-X} [NF_2] (1 - \phi_a) \sigma_{249} [NF_2] \quad (7)$$

where F_{a-X} and F_{b-X} are constants containing detection efficiency, geometries, and appropriate conversion factors; ϕ_a is the NF(a) photolysis quantum yield; σ_{249} is the NF_2 absorption cross section at 249 nm; I_{249} is the KrF photolysis flux in photons/cm²; and $[NF_2]$ is the NF_2 number density. Similar expressions can be written for the flux normalized signal amplitudes from ArF photolysis of HBr in the presence of NF_2 :

$$S'_{a-X}/I_{193} = F'_{a-X} B_a \sigma_{193} [HBr] \quad (8)$$

$$S'_{b-X}/I_{193} = F'_{b-X} (1-B_a) \sigma_{193} [HBr] \quad (9)$$

where F'_{a-X} and F'_{b-X} are similar to the constants F_{a-X} and F_{b-X} appearing in Eqs. (6) and (7), B_a is the NF(a) branching ratio, σ_{193} is the HBr absorption cross section at 193 nm, I_{193} is the ArF photolysis flux in photons/cm², and $[HBr]$ is the HBr number density. Equations (6) and (7) are valid under the assumption that the NF_2 photolysis quantum yield is unity, discussed in the previous section. Equations (8) and (9) assume that each H atom reacts with NF_2 in addition to taking the HBr photolysis quantum yield to be unity. At our typical operating temperatures of 420 K, the rate constant for the reaction of H atoms with HBr ($k_{420} = 5.9 \times 10^{-12}$ cm³/molecule-sec)^{29,30} is more than a factor of 2 slower than that for H + NF_2 ⁷ ($k = 1.30 \times 10^{-11}$ cm³/molecule-sec).^{5,7} Furthermore, for the work reported here, the HBr/ NF_2 ratios were kept at values so that at least 80% of the H atoms react with NF_2 . This point is discussed further below.

If no change is made in the excitation and detection geometries when signal amplitudes are measured for both KrF and ArF laser photolysis, then $F'_{b-X} = F_{b-X}$ and $F'_{a-X} = F_{a-X}$, and one obtains the following:

$$R_a = (\phi_a \sigma_{249} I_{249}) / (B_a \sigma_{193} I_{193}) \quad (14)$$

$$R_b = [(1 - \phi_a) \sigma_{249} I_{249}] / [(1 - B_a) \sigma_{193} I_{193}] \quad (15)$$

where R_a and R_b are the ratios $(S_{a-X}/I_{249})/(S'_{a-X}/I_{193})$ and $(S_{b-X}/I_{249})/(S'_{b-X}/I_{193})$, respectively. Solving for B_a and ϕ_a , one obtains

$$B_a = (1 - R_b \rho) / [\rho(R_a - R_b)] \quad (16)$$

$$\phi_a = (1 - R_b \rho) / (1 - R_b/R_a) \quad (17)$$

where $\rho = \sigma_{193}/\sigma_{249}$ is the ratio of the HBr absorption cross section at 193 nm and the NF_2 absorption cross sections at 249 nm.

In separate experiments, KrF photolysis of NF_2 and ArF photolysis of HBr/ NF_2 mixtures, the NF b-X LIF and NF a-X emission signals were recorded as a function of $[NF_2]$ and $[HBr]$, respectively. The b-X (0,0) $Q_P(9)/Q_R(9)$ line was probed with the dye laser. The addition of 5 Torr SF_6 ensured that the NF(X) state vibrational and rotational distributions were relaxed.²² In addition, 5 Torr CO_2 was also present to quench vibrationally excited HF produced in the $H + NF_2$ reaction.^{7,31} This effectively prevents any energy pooling^{1,27} between $HF(v) + NF(a)$ to produce $NF(b)$, which would contribute to the background signal. The NF(a) emission and NF b-X LIF time profiles were normalized for excimer laser flux. In addition, the b-X LIF signal was also normalized for the dye laser energy to correct for dye laser power fluctuations during the course of the measurements. In order to ensure that the experimental signals were indeed proportional to laser energy, NF(a) emission and NF b-X LIF were recorded as a function of laser flux in additional experiments. Figure 3 displays plots of NF b-X LIF intensity as a function of KrF and dye laser energy. Linear behavior is observed, and both plots extrapolate

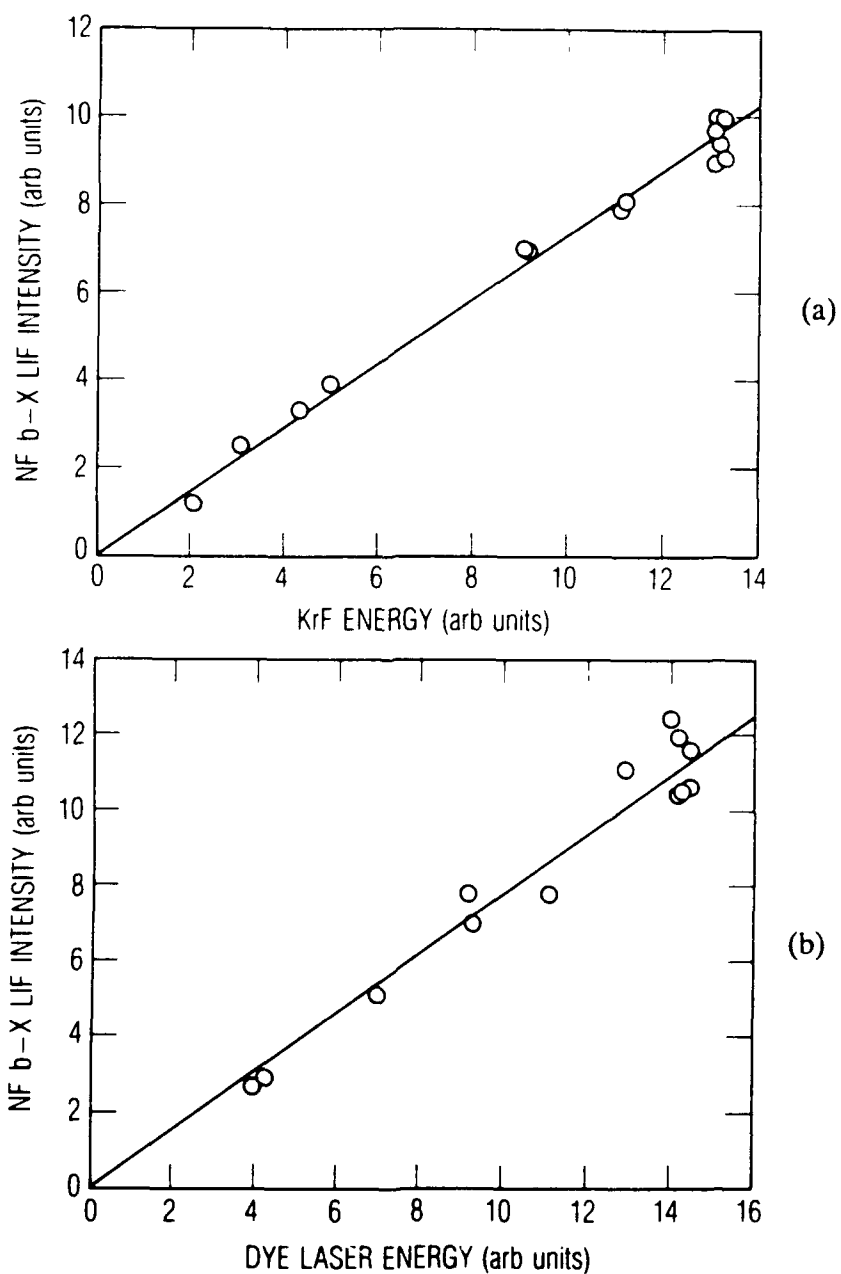
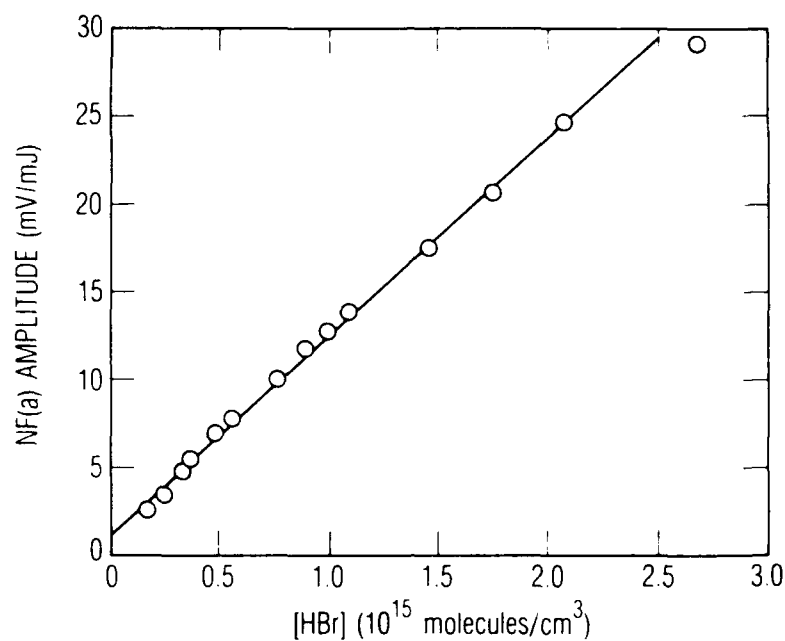


Fig. 3. Plots of the NF b-X LIF Intensity as a Function of Laser Energy. The dye laser was tuned to excite the $Q_P(9)/Q_R(9)$ line of the (0,0) band, and the delay between the KrF photolysis laser and dye laser was fixed at 100 μ sec. (a) shows the dependence of the LIF intensity upon the KrF laser energy, while (b) shows the variation with dye laser energy.

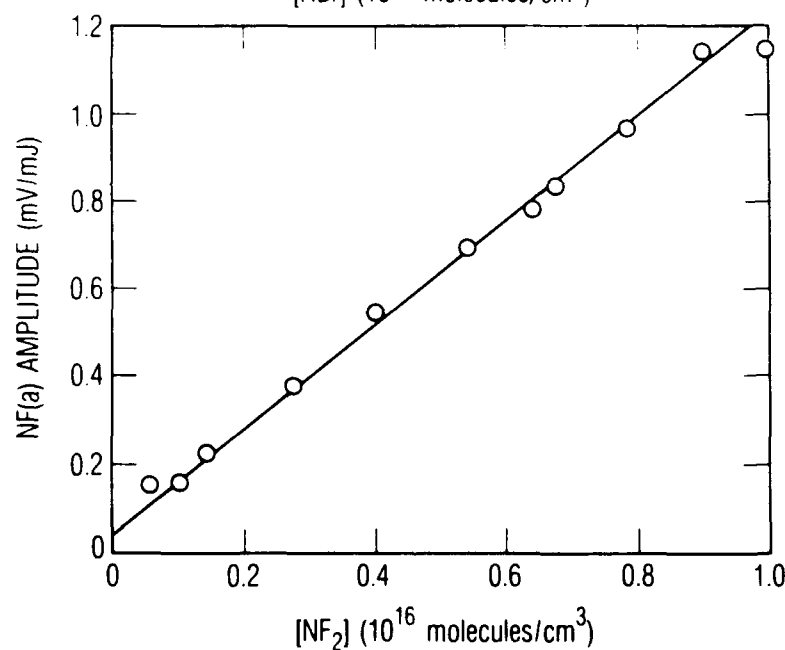
to zero. The same result was obtained for the NF(a) emission for both the KrF and ArF cases.

The experimental NF(a) and NF b-X time profiles were fit to a single exponential decay, and amplitudes were obtained from an extrapolation to time = 0. Plots for NF(a) amplitudes are shown in Fig. 4, and Fig. 5 contains a plot of the NF b-X LIF amplitude as a function of NF₂ density. In all cases the plots are linear. However, we were not able to observe any NF b-X LIF signal from the ArF photolysis of HBr/NF₂ mixtures. An NF b-X signal was searched for, using two different methods, and the results are displayed in Fig. 6. Also shown for comparison is the LIF observed from the KrF laser photolysis of NF₂ alone. In one experiment, the dye laser was tuned to excite the (0,0) Q_P(9)/Q_R(9) line, and the delay between the ArF and dye lasers was scanned. In another experiment, the time delay between the two lasers was held fixed, and the wavelength of the dye laser was varied. No b-X LIF could be detected in either case.

Since the strong LIF occurs at the same wavelength as the dye laser, it was necessary to use a gated detector (see experimental section), and thus a delay, Δt , is introduced between the time the dye laser excites the LIF and the time the LIF is detected. Hence, the b-X LIF amplitudes obtained from experimental data must be corrected by the factor $e^{k'\Delta t}$, where k' is the NF(b) removal rate. For the case of 249 nm photolysis, this factor is very close to unity since NF(b) quenching rate constants are very small for the species present.^{27,28} One would expect a similar situation for the 193 nm photolysis experiments since the additional reagent, HBr, does not efficiently remove NF(b) ($k_q = 5.7 \times 10^{-14}$ cm³/molecule-sec).²⁸ However, under our operating conditions, the observed NF(b) removal rates were several orders of magnitude faster than could be accounted for from known NF(b) quenching rate constants.^{27,28} We also observed that the NF(b) removal rate depended strongly upon the ArF photolysis laser pulse repetition rate. The NF(b) removal rate does indeed approach that calculated from known removal rate coefficients as the ArF repetition rate is decreased. Hence, the rapid NF(b) removal is due to the buildup of photolysis and reaction products at the higher repetition rates. The most probable species responsible for the fast



(a)



(b)

Fig. 4. (a) Plot of the NF(a) Amplitude from the 193 nm Photolysis of HBr in the Presence of NF₂. The NF₂ concentration was held constant at 3.9×10^{15} molecules/cm³ with SF₆ = 1.7×10^{17} molecules/cm³, Ar = 2.0×10^{16} , and CO₂ = 1.1×10^{17} molecules/cm³. Also shown in a linear fit to the data. (b) Plot of the NF(a) Amplitude from the 249 nm Photolysis of NF₂. Buffer gases densities were SF₆ = 1.7×10^{17} molecules/cm³, Ar = 2.0×10^{16} , and CO₂ = 1.1×10^{17} molecules/cm³. Also shown in a linear fit to the data.

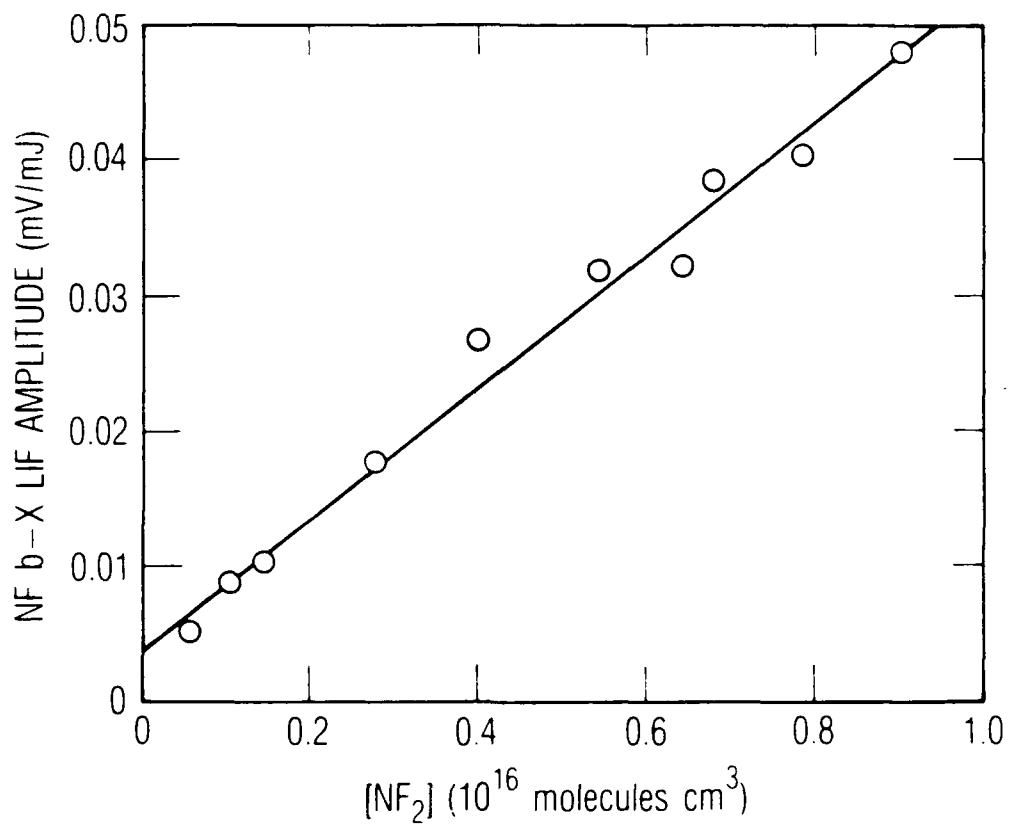


Fig. 5. Plot of the NF b-X LIF Amplitude as a Function of [NF₂] from the KrF Laser Photolysis of NF₂. Other species densities were SF₆ = 1.8 × 10¹⁷ molecules/cm³, Ar = 2.0 × 10¹⁶, and CO₂ = 1.1 × 10¹⁷ molecules/cm³. A linear fit to the data is indicated.

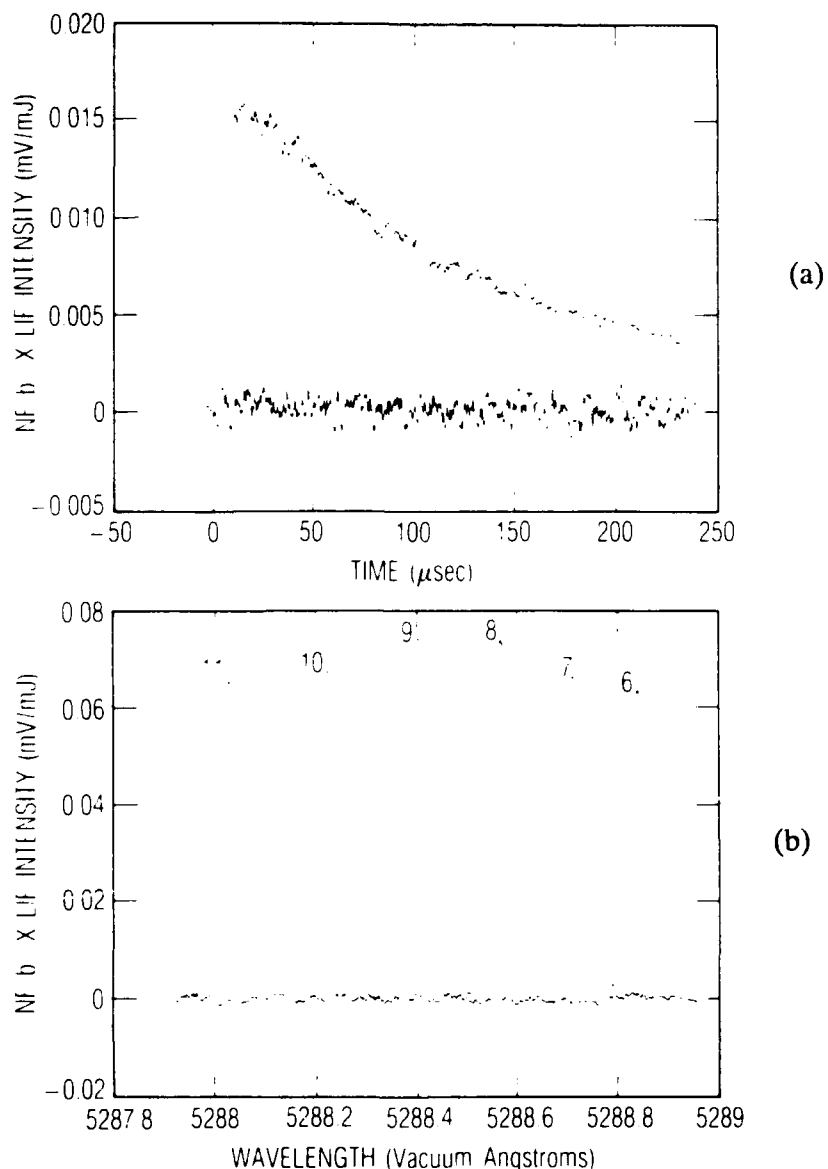


Fig. 6. (a) Time Profiles of NF b-X LIF Intensity Obtained by Tuning the Dye Laser to the $Q_P(9)/Q_R(9)$ Line of the (0,0) Band and Varying the Delay Between the Excimer Laser and Dye Laser Pulses. The large signal is from the KrF laser photolysis of NF_2 , while the other trace is from the ArF photolysis of an HBr/ NF_2 mixture. Experimental conditions for the KrF case had $NF_2 = 1.2 \times 10^{16}$ molecules/cm³, $SF_6 = 1.0 \times 10^{17}$ molecules/cm³, Ar = 6.2×10^{16} , and $CO_2 = 1.3 \times 10^{17}$ molecules/cm³. The ArF data had HBr = 3.3×10^{15} molecules/cm³, $NF_2 = 7.7 \times 10^{16}$ molecules/cm³, $SF_6 = 8.2 \times 10^{16}$ molecules/cm³, Ar = 8.0×10^{16} , and $CO_2 = 1.0 \times 10^{17}$ molecules/cm³. (b) NF b-X Excitation Spectra Obtained by Fixing the Delay Between the Excimer and Dye Lasers to 15 μ sec and Scanning the Dye Laser Wavelength. The spectrum is a portion of the b-X (0,0) band, and the strong Q_P/Q_R branch is labeled with the N'' rotational quantum number. The larger signal is from the KrF laser photolysis of NF_2 , while the other signal is from the ArF photolysis of an HBr/ NF_2 mixture. Conditions for the KrF case were $NF_2 = 2.8 \times 10^{15}$ molecules/cm³, $SF_6 = 1.8 \times 10^{17}$ molecules/cm³, Ar = 8.7×10^{16} , and $CO_2 = 1.2 \times 10^{17}$ molecules/cm³. The ArF data had HBr = 1.9×10^{15} molecules/cm³, $NF_2 = 3.9 \times 10^{15}$ molecules/cm³, $SF_6 = 1.7 \times 10^{17}$ molecules/cm³, Ar = 3.4×10^{16} , and $CO_2 = 1.1 \times 10^{17}$ molecules/cm³.

NF(b) removal is Br_2 , which removes NF(b) with a nearly gas kinetic rate constant²⁴ ($k = 1.4 \times 10^{-10} \text{ cm}^3/\text{molecule-sec}$). Such an extremely large rate coefficient indicates that NF(b) is removed by reaction with HBr rather than by energy transfer. This conclusion is supported by the fact that no $\text{NF}(X^3 \Sigma^-)$, produced from NF(b) quenching, is observed at later times. Duty cycle limitations precluded experiments from being performed at low ArF repetition rates ($<1 \text{ Hz}$) where the NF(b) removal was slow. We determined an empirical NF(b) removal rate constant at our operating conditions ($k' = 2 \times 10^{-11} \text{ cm}^3/\text{molecule-sec} \times [\text{HBr}]$) to be used in the extrapolation of the NF(b) signal at $t = 0$ with the factor $e^{k'\Delta t}$ given above.

A possible explanation of the absence of an NF b-X LIF signal from the ArF laser photolysis of HBr/NF₂ mixtures is that the NF ground state is removed by reaction with HBr. We studied the time behavior of the $\text{NF}(X^3 \Sigma^-)$ state from the 249 nm photolysis of NF₂ with HBr present and found no HBr dependence of its removal rate. Figure 7 shows two time profiles of the NF b-X LIF with and without added HBr. Although the observed NF b-X LIF intensity decreased with the addition of HBr due to the removal of NF(b) as discussed above, the NF(X) removal rate was not affected. Thus we conclude the absence of an NF b-X LIF signal from the 193 nm photolysis experiments is not due to removal by HBr or photolysis products but is a consequence of the extremely low $\text{H} + \text{NF}_2 \rightarrow \text{NF}(X) + \text{H}$ branching fraction.

Table 1 summarizes the results of two separate experiments in the determination of the $\text{H} + \text{NF}_2$ branching ratio. Tabulated slopes are obtained from plots of NF(a) emission and NF b-X LIF amplitudes vs NF₂ and HBr density. In addition, upper limits for the LIF amplitudes for ArF laser photolysis of HBr/NF₂ mixtures are presented. Equations (14)-(17) were employed to calculate the NF(a) branching ratio and NF(a) photolysis quantum yield. The NF₂ absorption cross section at 249 nm reported in Ref. 18, $\sigma = 6.74 \times 10^{-19} \text{ cm}^2$, and the HBr value at 193 nm given by Magnotta et al.³², $1.9 \times 10^{-18} \text{ cm}^2$, were used in the calculation.

Since we were unable to detect any NF(X) from the $\text{H} + \text{NF}_2$ reaction, the values for the NF(a) branching fraction and photolysis quantum yield displayed

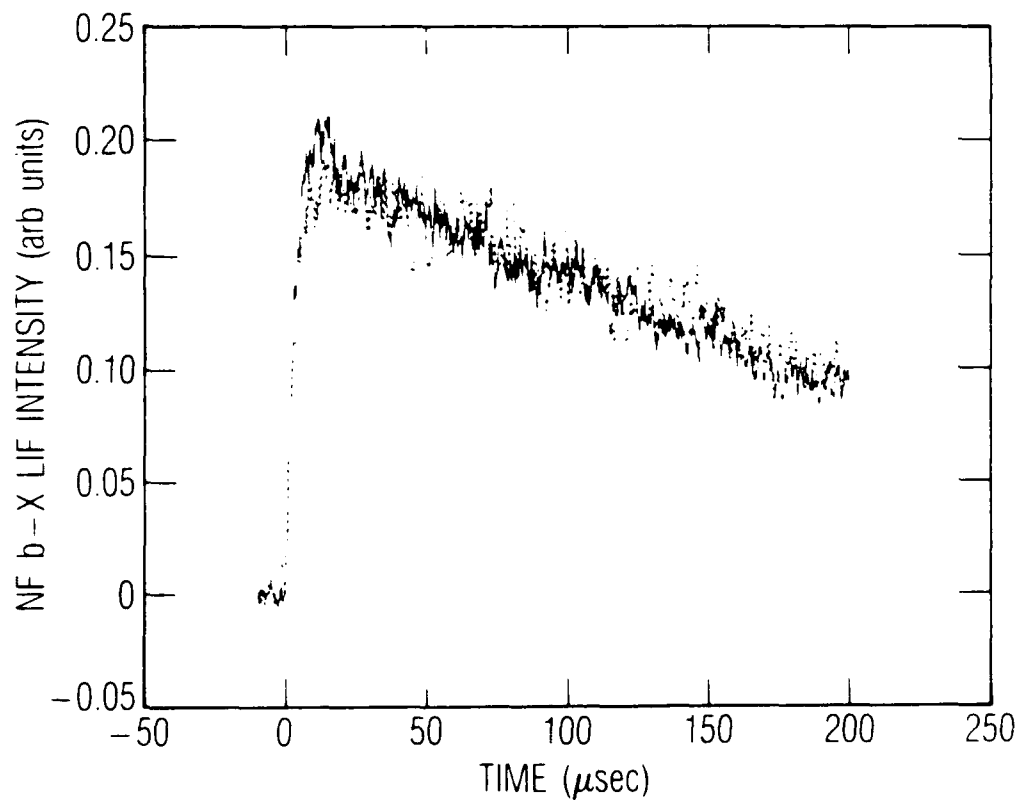


Fig. 7. Time Profiles of NF b-X LIF Intensity Obtained by Tuning the Dye Laser to the $Q_P(9)/Q_R(9)$ Line of the (0,0) Band and Varying the Delay Between the Excimer Laser and Dye Laser Pulses. The solid line is from the KrF laser photolysis of 1.0×10^{15} molecules/cm³ NF₂ with no HBr, while the dotted curve is the time profile with [HBr] = 4.1×10^{14} molecules/cm³ and the same NF₂ density. Other species were SF₆ = 3.0×10^{17} molecules/cm³ and Ar = 3.0×10^{16} .

Table 1. Experimental NF b-X LIF and a-X Emission Amplitudes vs Density^(a)

Process	Experimental Values ^(b)	
	Run #1	Run #2
NF ₂ + hv (249 nm) → NF(a) + F	2.1(0.4) × 10 ⁻³¹	9.5(1.8) × 10 ⁻³²
NF ₂ + hv (249 nm) → NF(X) + F	6.2(1.2) × 10 ⁻³³	3.8(0.8) × 10 ⁻³³
NF ₂ + H → NF(a) + F ^(c)	8.6(1.7) × 10 ⁻³⁰	7.1(1.4) × 10 ⁻³⁰
NF ₂ + H → NF(X) + F ^(c)	< 2 × 10 ^{-33(d)}	< 1.0 × 10 ^{-33(d)}
<hr/>		
NF(a) Branching Fraction ^(e)	> 0.90 ± 0.03	> 0.9 ± 10.03
NF(a) 249 nm Photolysis Quantum Yield ^(e)	< 0.06 ± 0.02	< 0.03 ± 0.01

(a) Given by Eqs. (6)-(9).

(b) Values given have units of cm³-mV/molecule-photon. Estimated uncertainties (2σ) given in parentheses.

(c) H atoms produced from the 193 nm photolysis of HBr.

(d) Estimated upper limit using an empirical NF(b) removal rate constant by HBr of 2 × 10⁻¹¹ cm³/molecule-sec (see text).

(e) Calculated from Eqs. (16) and (17). The uncertainties, given in parentheses, are calculated from an error propagation analysis using the estimated 2σ errors in the experimental data.

in Table 1 are lower and upper limits, respectively. The relative magnitudes of the ratios R_a and R_b , appearing in Eqs. (16) and (17), make the calculation of the branching fraction and quantum yield very insensitive to relatively large changes in the experimental data used to perform the calculation. This is a consequence of the fact that the NF(a) 249 nm quantum yield is very low, while the NF(a) branching fraction is near unity, making R_a a large number and R_b small. For example, a factor of 2 change in any of the four parameters used to determine the branching fraction results in only a $\pm 10\%$ change in the result. Results from rigorous propagation of errors calculation were used to determine the uncertainty in the NF(a) branching and quantum yield. It is interesting to note that the calculated errors in the branching fraction and the quantum yield are only 15% and 144%, respectively, if one takes the errors in the four experimental parameters in Table 1 to be of the same magnitude as the parameters themselves.

IV. CONCLUSIONS

The ability to directly monitor the NF(X) state using LIF on the NF b-X transition has been applied to an absolute measurement of the H + NF₂ branching ratio and the NF₂ photolysis quantum yield. An analysis of the NF b-X LIF and NF a-X emission produced from both the KrF photolysis of NF₂ and the 193 nm photolysis of HBr in NF₂ results in a lower limit for the H + NF₂ → NF(a) + HF branching ratio of 0.90 ± 0.03 , in good agreement with previous results.⁵⁻⁷ In addition, the NF(a) photolysis quantum yield at 249 nm reported here agrees with prior work performed in this laboratory.¹⁷

REFERENCES

1. J. M. Herbelin and N. Cohen, Chem. Phys. Lett. 20, 605 (1973).
2. M. A. A. Clyne and I. F. White, Chem. Phys. Lett. 6, 465 (1970).
3. D. L. King and D. W. Setser, Ann. Rev. Phys. Chem. 27, 407 (1976).
4. J. M. Herbelin, Chem. Phys. Lett. 42, 367 (1976).
5. C. T. Cheah, M. A. A. Clyne, and P. D. Whitefield, J. Chem. Soc. Faraday Trans. II 76, 711 (1980).
6. C. T. Cheah and M. A. A. Clyne, J. Chem. Soc. Faraday Trans. II 76, 1543 (1980).
7. R. J. Malins and D. W. Setser, J. Phys. Chem. 85, 1342 (1981).
8. F. E. Hovis, P. D. Whitefield, H. V. Linenfeld, and G. R. Bradburn, J. Phys. Chem. 92, 5133 (1988).
9. F. A. Johnson and C. B. Colburn, J. Am. Chem. Soc. 83, 3043 (1961).
10. A. P. Modica and D. F. Hornig, J. Chem. Phys. 49, 629 (1968).
11. S. N. Foner and R. L. Hudson, J. Chem. Phys. 58, 581 (1973).
12. P. J. Evans and E. Tschuikow-Roux, J. Chem. Phys. 65, 4202 (1976).
13. P. J. Evans and E. Tschuikow-Roux, J. Phys. Chem. 82, 182 (1978).
14. P. H. Tennyson, A. Fontijn, and M. A. A. Clyne, Chem. Phys. 62, 171 (1981).
15. A. E. Douglas and W. E. Jones, Can. J. Phys. 44, 2251 (1966).
16. M. Vervloet and J. K. G. Watson, Can. J. Phys. 64, 1529 (1986).
17. J. B. Koffend, C. E. Gardner, and R. F. Heidner III, J. Chem. Phys. 83, 2904 (1985).
18. R. F. Heidner, H. Helvajian, and J. B. Koffend, J. Chem. Phys. 87, 1520 (1987).
19. P. L. Goodfriend and H. P. Woods, J. Mol. Spectrosc. 13, 63 (1964).
20. L. A. Kuznetsova, Y. Y. Kuzyakov, and V. M. Tatevskii, Opt. Spectrosc. 16, 295 (1964).

REFERENCES (Continued)

21. D. G. Imre, J. L. Kinsey, R. W. Field, and D. H. Kayatama, 7th International Symposium on Gas Kinetics, Gottingen, 1982.
22. R. F. Heidner, H. Helvajian, J. S. Holloway, and J. B. Koffend (to be published).
23. M. A. A. Clyne and W. S. Nip, Int. J. Chem. Kinet. X, 367 (1978).
24. H. Cha and D. W. Setser, J. Phys. Chem. 91, 3658 (1987).
25. M. A. Kwok, J. M. Herbelin, and N. Cohen, "Electronic Transition Lasers I", J. Steinfeld, Ed., MIT Press, Cambridge, MA.
26. P. H. Tennyson, A. Fontijn, and M. A. A. Clyne, Chem. Phys. 62, 171 (1981).
27. D. Lin and D. W. Setser, J. Phys. Chem. 89, 1561 (1985).
28. H. Cha and D. W. Setser (to be published).
29. H. Endo and G. P. Glass, J. Phys. Chem. 80, 1519 (1976).
30. D. L. Baulch, J. Duxbury, S. J. Grant, and D. C. Montague, J. Phys. Chem. Ref. Data 10, (1981).
31. J. F. Bott, J. Chem. Phys. 65, 4239 (1976).
32. F. Magnotta, D. J. Nesbitt, and S. R. Leone, Chem. Phys. Lett. 83, 21 (1981).

LABORATORY OPERATIONS

The Aerospace Corporation functions as an "architect-engineer" for national security projects, specializing in advanced military space systems. Providing research support, the corporation's Laboratory Operations conducts experimental and theoretical investigations that focus on the application of scientific and technical advances to such systems. Vital to the success of these investigations is the technical staff's wide-ranging expertise and its ability to stay current with new developments. This expertise is enhanced by a research program aimed at dealing with the many problems associated with rapidly evolving space systems. Contributing their capabilities to the research effort are these individual laboratories:

Aerophysics Laboratory: Launch vehicle and reentry fluid mechanics, heat transfer and flight dynamics; chemical and electric propulsion, propellant chemistry, chemical dynamics, environmental chemistry, trace detection; spacecraft structural mechanics, contamination, thermal and structural control; high temperature thermomechanics, gas kinetics and radiation; cw and pulsed chemical and excimer laser development, including chemical kinetics, spectroscopy, optical resonators, beam control, atmospheric propagation, laser effects and countermeasures.

Chemistry and Physics Laboratory: Atmospheric chemical reactions, atmospheric optics, light scattering, state-specific chemical reactions and radiative signatures of missile plumes, sensor out-of-field-of-view rejection, applied laser spectroscopy, laser chemistry, laser optoelectronics, solar cell physics, battery electrochemistry, space vacuum and radiation effects on materials, lubrication and surface phenomena, thermionic emission, photosensitive materials and detectors, atomic frequency standards, and environmental chemistry.

Electronics Research Laboratory: Microelectronics, solid-state device physics, compound semiconductors, radiation hardening; electro-optics, quantum electronics, solid-state lasers, optical propagation and communications; microwave semiconductor devices, microwave/millimeter wave measurements, diagnostics and radiometry, microwave/millimeter wave thermionic devices; atomic time and frequency standards; antennas, rf systems, electromagnetic propagation phenomena, space communication systems.

Materials Sciences Laboratory: Development of new materials: metals, alloys, ceramics, polymers and their composites, and new forms of carbon; nondestructive evaluation, component failure analysis and reliability; fracture mechanics and stress corrosion; analysis and evaluation of materials at cryogenic and elevated temperatures as well as in space and enemy-induced environments.

Space Sciences Laboratory: Magnetospheric, auroral and cosmic ray physics, wave-particle interactions, magnetospheric plasma waves; atmospheric and ionospheric physics, density and composition of the upper atmosphere, remote sensing using atmospheric radiation; solar physics, infrared astronomy, infrared signature analysis; effects of solar activity, magnetic storms and nuclear explosions on the earth's atmosphere, ionosphere and magnetosphere; effects of electromagnetic and particulate radiations on space systems; space instrumentation.